# Radical Pair Dynamics and Interactions in Quinone-Reconstituted Photosynthetic Reaction Centers of *Rb. sphaeroides* R26: A Multifrequency Magnetic Resonance Study

**R. J. Hulsebosch, I. V. Borovykh, S. V. Paschenko, P. Gast, and A. J. Hoff***

*Department of Biophysics, Huygens Laboratory, Leiden University, P.O. Box 9504, 2300 RA Leiden, The Netherlands*

*Received: February 24, 1999; In Final Form: May 5, 1999*

The secondary photoinduced radical pair state $P^{+\bullet}\,Q_A^{-\bullet}$ in Zn-substituted and quinone-reconstituted photosynthetic reaction centers of *Rhodobacter sphaeroides* R26 is investigated with transient EPR spectroscopy at X- (9.3 GHz), Q- (34.7 GHz), and D-band (130.0 GHz) microwave frequencies. Novel D-band $P^{+\bullet}\,Q_A^{-\bullet}$ electron spin-polarized spectra are presented for three different reconstituted reaction centers. The shape of the electron spin-polarized $P^{+\bullet}\,Q_A^{-\bullet}$ EPR spectrum strongly depends on the lifetime and magnetic properties of its precursor radical pair $P^{+\bullet}\,\Phi_A^{-\bullet}$, whose lifetime was manipulated by replacing the native ubiquinone-10 (UQ-10) with duroquinone (DQ) or 2-ethyl anthraquinone (AQ). From spectral simulations incorporating the transfer of spin-correlation between the two radical pairs, information about the magnetic interactions and dynamics of the intermediate primary $P^{+\bullet}\,\Phi_A^{-\bullet}$ radical pair was obtained. When the lifetime of $P^{+\bullet}\,\Phi_A^{-\bullet}$ is longer than a few nanoseconds, the influence of the magnitude and sign of the exchange interaction $J_{P\Phi}$ between $P^{+\bullet}$ and $\Phi_A^{-\bullet}$ on the shape of the observed ESP spectrum is significant. This effect is even more pronounced at the relatively high D-band microwave frequency, facilitating accurate determination of $J_{P\Phi} = -0.9 \pm 0.1$ mT, for both DQ and AQ-reconstituted RCs, a value not significantly different from that determined here for the UQ-10 reconstituted sample ($J_{P\Phi} = -0.7 \pm 0.5$ mT). The singlet and triplet rate constants ($k_S$ and $k_T$) for the intermediate radical pair $P^{+\bullet}\,\Phi_A^{-\bullet}$ in the duroquinone- or 2-ethyl anthraquinone-reconstituted samples were $(2 \pm 1) \times 10^7$ $s^{-1}$ and $(2 \pm 1) \times 10^8$ $s^{-1}$, respectively. The exchange interaction between $P^{+\bullet}$ and $\Phi_A^{-\bullet}$ is $J_{PQ} = -0.5 \pm 0.3$ $\mu$T, $-0.2 \pm 0.1$ $\mu$T, and $-0.5 \pm 0.2$ $\mu$T for UQ-10, AQ, and DQ, respectively. X-band ESEEM experiments showed that the dipolar interaction between $P^{+\bullet}$ and $\Phi_A^{-\bullet}$ is $-0.12 \pm 0.01$ mT, independent of the quinone, corresponding to a center-to-center distance of $28.5 \pm 0.8$ Å.

## 1. Introduction

Excitation of the primary electron donor P, a bacteriochlorophyll dimer, in photosynthetic reaction centers (RCs) of purple bacteria triggers a series of electron-transfer events:

$$P\Phi_A Q_A Q_B \xrightarrow{h\nu} P^*\Phi_A Q_A Q_B \xrightarrow{k_\Phi} P^{+\bullet}\,\Phi_A{}^{-\bullet} Q_A Q_B \xrightarrow{k_Q} P^{+\bullet}\,\Phi_A Q_A{}^{-\bullet} Q_B \xrightarrow{k_{AB}} P^{+\bullet}\,\Phi_A Q_A Q_B{}^{-\bullet} \rightarrow \ldots$$

where $\Phi_A$ and $Q_A$ are a bacteriopheophytin and the primary electron acceptor quinone, respectively. Each state is characterized by a forward electron transfer rate $k$. In the native system, $k_\Phi = 2.5 \times 10^{11}$ $s^{-1}$, $k_Q = 5.0 \times 10^9$ $s^{-1}$, and the electron transfer rate from $Q_A^{-\bullet}$ to the secondary quinone $Q_B$ is $k_{AB} = 5.0 \times 10^3$ $s^{-1}$ at room temperature (for a review see ref 1). The secondary radical pair (RP) $P^{+\bullet}\,Q_A^{-\bullet}$ has been studied extensively by time-resolved electron paramagnetic resonance (EPR) spectroscopy (recently reviewed in ref 2). The transient EPR spectrum of $P^{+\bullet}\,Q_A^{-\bullet}$ shows a high degree of electron spin polarization (ESP) at early times. Interpretation of experimental ESP spectra with the spin-correlated radical pair (SCRP) model[3,4] has yielded valuable information about the mutual orientation and the magnetic and electronic interactions of both radicals. The latter two are difficult to assess with any other technique, and especially the magnetic exchange interaction is of direct relevance to understanding photoinduced electron transfer.[5−7] In most of the ESP studies, the lifetime of the primary RP, $P^{+\bullet}\,\Phi_A^{-\bullet}$, was assumed to be much shorter than the time scale corresponding to its magnetic interactions. Thus, the observed secondary RP was considered to be initially in a pure singlet state and any admixture of triplet character was ignored. Under certain conditions, however, the lifetime of the $P^{+\bullet}\,\Phi_A^{-\bullet}$ state may be prolonged, resulting in a more pronounced singlet−triplet interconversion under the influence of the dipolar, exchange, hyperfine, and Zeeman interactions of the two radicals. The initial state of the subsequently formed secondary SCRP, $P^{+\bullet}\,Q_A^{-\bullet}$, then will no longer be a pure singlet state, with quite dramatic effects on the ESP line shape. For a complete characterization of the magnetic properties of $P^{+\bullet}\,Q_A^{-\bullet}$, one needs therefore to consider the singlet and triplet decay rates of $P^{+\bullet}\,\Phi_A^{-\bullet}$ ($k_S$ and $k_T$) as well as the singlet−triplet mixing frequencies ($2Q_{1,2}$) together with the dipolar and exchange interactions of *both* $P^{+\bullet}\,\Phi_A^{-\bullet}$ and $P^{+\bullet}\,Q_A^{-\bullet}$. The RP energy level scheme and its corresponding EPR transitions are shown in Scheme 1. Here, the isotropic exchange interaction, $2J$, is defined as the energy difference $E(S) - E(T_0)$ between the singlet and triplet RP states.

Several models that extend the existing SCRP mechanism with a contribution of an intermediate RP have been described.[8−11] Experimental data on the effect of an intermediate RP, however, is scant and pertains only to $Fe^{2+}$-containing RCs.[10,12] We have

* Corresponding author. Phone: +31-71-5275955. Fax: +31-71-5275819. E-mail: hoff@biophys.leidenuniv.nl.

10.1021/jp990677c CCC: $18.00 
Published on Web 07/23/1999

**SCHEME 1: Transfer of Spin-Correlation between RPs in the Photosynthetic RC, the RP Energy Level Scheme, and the Corresponding EPR Transitions**

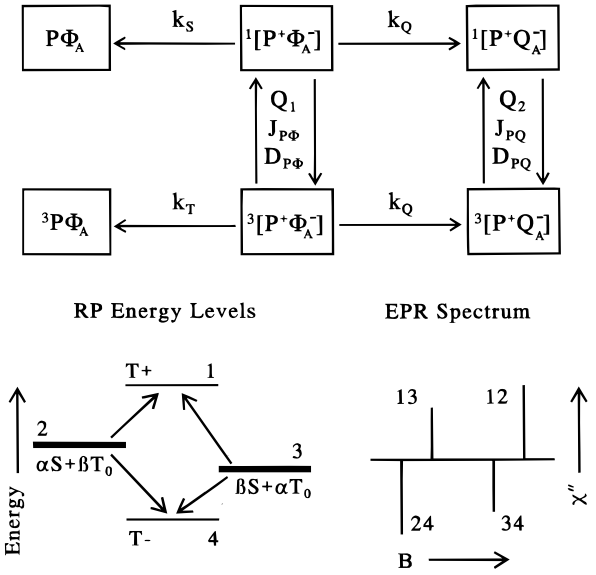


therefore endeavored to experimentally assess effects of a relatively long-lived primary $P^{+\bullet}\,\Phi_A^{-\bullet}$ RP state in well-characterized RC preparations.

Three methods are known to reduce the rate of formation of the secondary RP $P^{+\bullet}\,Q_A^{-\bullet}$ in bacterial RCs: $Fe^{2+}$ removal,[13−15] quinone substitution,[10,16,17] or site-specific mutagenesis.[18,19] It is known that upon removal of the paramagnetic $Fe^{2+}$ atom and in the presence of the H-subunit, the lifetime of $P^{+\bullet}\,\Phi_A^{-\bullet}$ is reduced by a factor of 50.[13,15] The disadvantage of this rather crude method is that it causes severe alterations of the quinone binding site,[20] which may be related to the prolongation of the $P^{+\bullet}\,\Phi_A^{-\bullet}$ RP lifetime. Zn substitution essentially restores the kinetics[13] of the RC and the binding properties of the quinone.[20] The second option, replacement of the native quinone with quinones of different redox potentials, alters the free energy of $Q_A^{-\bullet}$ and therefore the electron transfer rates between $\Phi_A$ and $Q_A$ over a broad range.[10,16,17,21,22] Finally, site-specific mutations in the quinone binding sites of the RC caused a pronounced (10 times) slower sequential electron transfer between $\Phi_A^{-\bullet}$ and $Q_A$.[18,19]

The effects of sequential electron transfer on the ESP spectrum of $P^{+\bullet}\,Q_A^{-\bullet}$ in Fe-containing bacterial RCs with different quinones have been investigated.[10,23] The presence of the fast relaxing iron atom that is strongly coupled to the spin on the quinone radical gives rise to severe linebroadening and a *g*-value shift, resulting in a substantial decrease of the intensity of the quinone part of the RP resonances. In ref 10, a sequential electron transfer model was used for the spectral simulations but the considerable *g*-anisotropy of the $Fe^{2+}$-ion was not properly taken into account so that it is difficult to assess the conclusions drawn from the simulations.[24] Van der Est et al.[25] have reported 24 GHz ESP experiments with perdeuterated, Zn-containing RCs in which the native ubiquinone was replaced by duroquinone or naphthoquinone. Unfortunately, in the interpretation, transfer of spin-correlation between the primary and secondary radical pairs was neglected.

In this communication, we investigate the effect of the intermediate RP $P^{+\bullet}\,\Phi_A^{-\bullet}$ on the X- (9.31 GHz), Q- (34.67 GHz), and D-band (130.0 GHz) ESP spectra of $P^{+\bullet}\,Q_A^{-\bullet}$ for quinone-reconstituted, Zn-substituted RCs of *Rhodobacter (Rb.) sphaeroides* R26. Three specific quinones were selected to alter the $P^{+\bullet}\,\Phi_A^{-\bullet}$ lifetime: ubiquinone-10 (UQ-10, $E^{1}/_{2} = 110$ meV), duroquinone (2,3,5,6-tetramethyl benzoquinone, DQ, $E^{1}/_{2} = 30$ meV), and 2-ethyl anthraquinone (AQ, $E^{1}/_{2} = -245$ meV). UQ-10 was chosen to check the reconstitution procedure. The reduction rate for UQ-10 in RCs of *Rb. sphaeroides* is $k_Q = 5 \times 10^9\ s^{-1}$;[13] DQ shows an intermediate $k_Q$ of $3 \times 10^8\ s^{-1}$,[10,16] whereas AQ, with its large three-ring structure, produces a relatively small $k_Q$ of $4 \times 10^7\ s^{-1}$.[10,16]

For simulating the observed ESP spectra, we extended the simulation program based on the SCRP model[3,26] with the model of Hore to account for the lifetime of the primary RP $P^{+\bullet}\,\Phi_A^{-\bullet}$ and subsequent induced transfer of electron spin-correlation to the secondary RP $P^{+\bullet}\,Q_A^{-\bullet}$ (eqs 23 and 24 in ref 8). Furthermore, the recently described effect of magneto-photoselection on laser flash-induced ESP spectra was taken into account.[27] Novel transient ESP spectra at the D-band frequency demonstrate that especially at higher EPR frequencies the effects of a long-lived primary radical pair state on the ESP spectrum are dramatic. Simultaneously fitting the ESP spectra for three different EPR frequencies and three different acceptor quinones, we have obtained accurate information about the sign and magnitude of the exchange interaction between $P^{+\bullet}$ and $\Phi_A^{-\bullet}$: $J_{P\Phi} = -0.9 \pm 0.1$ mT for DQ- and AQ-reconstituted RCs and $-0.7 \pm 0.5$ mT for UQ-10-reconstituted RCs. Moreover, the singlet and triplet electron−hole recombination rates of the $P^{+\bullet}\,\Phi_A^{-\bullet}$ RP state, $k_S$ and $k_T$, and its rate of forward electron transport, $k_Q$, were determined from the fits of the ESP spectra of the various quinone-reconstituted samples; they agreed well with literature values. Out-of-phase electron spin−echo envelope modulation (ESEEM) experiments showed that the dipolar coupling between $P^{+\bullet}$ and $Q_A^{-\bullet}$ is $-0.12 \pm 0.01$ mT, independent of the type of quinone present in the $Q_A$ site.

The ESP studies in this work for the first time combine multifrequency time-resolved EPR, quinone replacement and polarized light excitation (magnetophotoselection). The simultaneous simulations of 15 ESP spectra are excellent and have yielded reliable values for the magnetic properties of the radical pairs $P^{+\bullet}\,\Phi_A^{-\bullet}$ and $P^{+\bullet}\,Q_A^{-\bullet}$.

## 2. Materials and Methods

Removal of the native ubiquinones from RCs of *Rb. sphaeroides* R26 and reconstitution of $Q_A$ with ubiquinone-10 (UQ-10, in 1% Triton X-100), duroquinone (DQ, in ethanol), or 2-ethyl anthraquinone (AQ, in ethanol) were performed according to ref 28. All quinones were purchased from Sigma. Prior to the reconstitution, the iron was removed.[29] Finally, $Zn^{2+}$ was added to occupy the vacant iron position. Quinone removal was better than 95%; $Q_A$ reconstitution with UQ-10, DQ, or 2-ethyl AQ was $90 \pm 5\%$, $90 \pm 5\%$, and $15 \pm 5\%$, respectively. The $Q_B$-pocket was partially occupied or not occupied. EPR samples with an $OD_{800}$ of 25 $cm^{-1}$, containing 60% v/v glycerol, were frozen in liquid nitrogen in the dark.

A Continuum Surelight I-pumped OPO laser was used for exciting the samples at different wavelengths. For the photoselection experiments, the originally vertically plane-polarized OPO light could be rotated to the horizontal plane using a set of two mirrors. A depolarizing light guide was used to perform nonphotoselection experiments. Time-resolved direct-detection X-band (Varian E-9, 9.31 GHz, 0.1 mW, 30 K) and Q-band (home-built, 34.67 GHz, 100 nW, 100 K) EPR experiments were carried out using boxcar integration of the signals with a sampling gate width of 1.5 $\mu$s and a 500 ns delay after the laser flash (DAF). Since the DAF is much longer than $k_Q^{-1}$, we can ignore the second-order effects discussed by Hore.[8] No photo-

selection was observed for the Q-band spectra since high laser power and a highly scattering silver-coated cylindrical cavity were used to obtain the spectra. D-band (130.0 GHz) ESP spectra were recorded with a pulsed spectrometer constructed in the Donetsk Physico-Technical Institute, Ukrainian National Academy of Sciences, Ukraine. The 130.0 GHz microwave bridge is based on a free running fixed-frequency source using an IMPATT oscillator amplifier in combination with a frequency tunable, single-mode cylindrical resonator ($TE_{011}$). Field-swept ESE spectra were recorded at 85 K with a two-pulse echo sequence (56 ns and 110 ns, $\tau = 190$ ns). Approximately 1.3 $\mu$s after laser excitation via a depolarizing light guide and fiber the intensity of the echo was probed with a 100 ns gated boxcar integrator (Princeton Applied Research, model 162). Excitation flashes were generated by a Spectron Laser Systems Nd:YAG laser (532 nm, half-width 6 ns, 10 Hz, 2 mJ/pulse).

Electron spin−echo measurements were carried out with a home-built X-band ESE spectrometer[30] at 100 K. A two-pulse sequence was used: laserflash−1.0 $\mu$s−pulse 1 (8 ns)−$\tau$−pulse 2 (16 ns)−$\tau$−echo. To acquire the ESEEM time-domain traces, the delay time $\tau$ was varied from 0.2 to 3.0 $\mu$s. In this two-pulse experiment, the light-induced RP causes an out-of-phase electron spin−echo that shows an envelope modulation. From the modulation frequencies information about the exchange and dipolar couplings can be derived.[31−33]

Simulations of the $P^{+\bullet}\,Q_A^{-\bullet}$ ESP spectra were performed according to the SCRP model.[3,26] This model was extended with the formalisms for transfer of spin-correlation between two radical pairs[8] and magnetophotoselection.[27] A W-band (95 GHz) single-crystal study[34] showed four possible orientations of the principal *g*-tensor components of $P^{+\bullet}$ in the crystallographic frame of reference. There has been some controversy on the use of the two most likely orientations, I or II, for $g_P$ in the ESP simulations. Simulations of X-[35] and K-band (24 GHz)[36,37] ESP spectra suggested that orientation I is to be preferred, whereas for W-band, orientation II yields better results.[38] According to Tang,[39] both orientations are applicable at X-, K-, and W-band if one allows small variations in the principal *g*-values of $P^{+\bullet}$ and $Q_A^{-\bullet}$ (which were considered "free" parameters). We prefer using experimentally determined principal *g*-values for $P^+$ from W-band EPR on single-crystals of *Rb. sphaeroides*.[34] For $Q_A^{-\bullet}$ the *g* values were determined from our D-band data using photoreduced RCs (data not shown). The orientation of the *g*-tensor of $Q_A^{-\bullet}$ and the direction of the $P^{+\bullet}\,Q_A^{-\bullet}$ and $P^{+\bullet}\,\Phi_A^{-\bullet}$ dipolar axis with respect to the crystallographic frame were calculated for ubiquinone in the native RC, using the crystal structure 4RCR.[40] We find that orientation II gives satisfactory simulations of the ESP spectra at all three EPR frequencies.

## 3. Results

Figures 1 and 2 show experimental and simulated photoselected and nonphotoselected X-, Q-, and D-band $P^{+\bullet}\,Q_A^{-\bullet}$ ESP spectra of various $Q_A$-reconstituted samples. The spectra of the UQ-10 reconstituted sample (Figures 1A and 2A) are virtually identical to the spectra obtained for protonated native (nonquinone replaced) Zn-substituted samples (for X-band see ref 27; for Q-band see ref 41). Clearly visible is the enhanced *g*-value resolution of $P^{+\bullet}$ and $Q_A^{-\bullet}$ as the microwave frequency increases. A relatively long lifetime for $P^{+\bullet}\,\Phi_A^{-\bullet}$ of 25 ns[13] is obtained when UQ-10 is replaced with 2-ethyl AQ. The amplitudes of the corresponding spectra (Figures 1B and 2B) are, when taking into account the low reconstitution efficiency, about 15 times larger than the UQ-10 spectra. This increase is

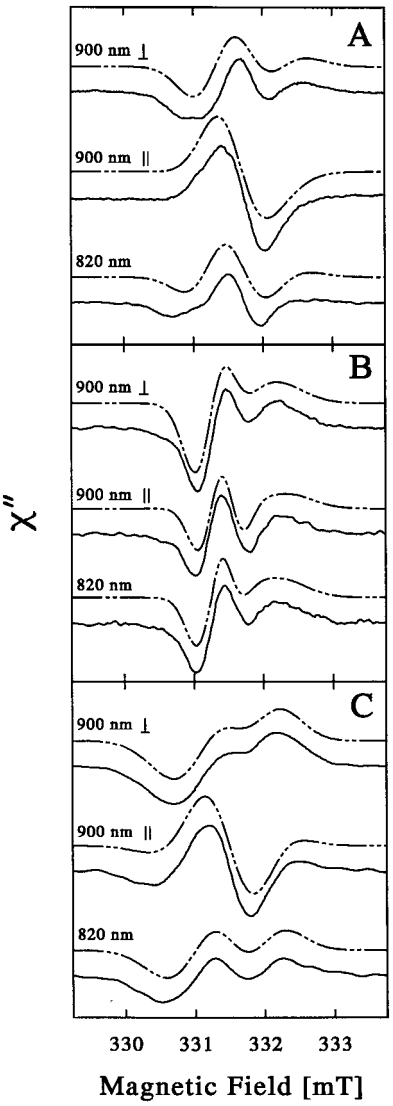


**Figure 1.** Experimental (solid lines) and simulated (dashed lines) (non)-photoselected X-band $P^{+\bullet}\,Q_A^{-\bullet}$ ESP spectra of $Q_A$-reconstituted, Zn-containing RCs of *Rb. sphaeroides* R26. $Q_A$ was reconstituted with (A) UQ-10, (B) 2-ethyl anthraquinone, and (C) duroquinone. Laser excitation at 900 nm, with the polarization of the light parallel and perpendicular to $B_0$, was used for photoselection experiments; excitation at 820 nm, via a depolarizing lightguide, was used for nonphotoselection experiments. $T = 30$ K.

partly caused by the narrow intrinsic line width of the AQ ($\Delta B_Q = 0.43 \pm 0.03$ mT) and partly by the low decay rate $k_Q$ (see discussion). The influence of photoselection is small. Simulations proved that the effect of photoselection is, to a large extent, neutralized by the narrow line width of AQ. For the duroquinone sample, severe linebroadening effects ($\Delta B_Q = 1.04 \pm 0.04$ mT), probably due to the increased amount of anisotropic proton hyperfine interactions from the four methyl groups, cause a drastic change of the ESP spectrum (Figures 1C and 2C). Nevertheless, the amplitudes of the spectra are similar to those of the UQ-10 spectra. Also, the effect of photoselection is clearly visible and well simulated. Baseline corrections were applied to account for the polarized primary donor triplet, $^3P$, arising from the remaining quinone-depleted RCs (about 80% for AQ and less than 5% for UQ-10 or DQ). The ESP signals from nonreconstituted quinone-containing RCs (about 5% for all samples) was subtracted. The parameters used for the spectral simulations are given in Table 1. The quinone line width contributions, $B_Q$, are in good agreement with the in vitro data

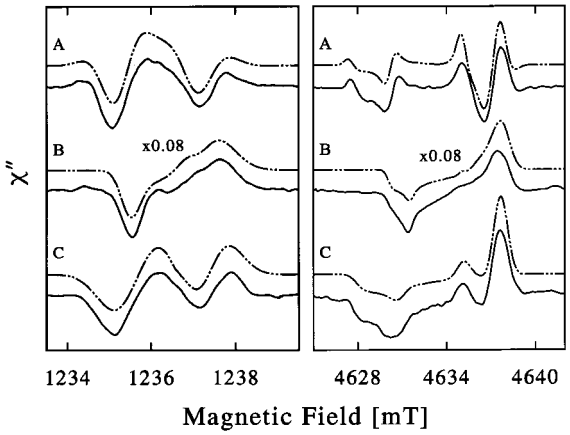


**Figure 2.** Experimental (solid lines) and simulated (dashed lines) nonphotoselected Q-band (left panel) and D-band (right panel) $P^{+\bullet}$ $Q_A^{-\bullet}$ ESP spectra of $Q_A$-reconstituted, Zn-containing RCs of *Rb. sphaeroides* R26. $Q_A$ is reconstituted with (A) UQ-10, (B) 2-ethyl anthraquinone (~15 times reduced in amplitude), and (C) duroquinone. Laser excitation at 820 nm was used for the Q-band spectra and at 532 nm for the D-band spectra. $T = 100$ K.

presented by Burghaus et al.,[42] whereas the small deviations in the principal $g$ values can be attributed to the different local environments. For example, hydrogen bond interactions with the carbonyl oxygens of the quinone radical are known to alter the $g_{xx}$ and $g_{yy}$ values.[43]

The $k_Q$ decay rates correspond well with the rates reported in refs 10 and 16, whereas the triplet decay rates, $k_T$, for the DQ and AQ reconstituted samples are somewhat smaller than the value for the native system determined from reaction yield detected magnetic resonance (RYDMR, for an overview see ref 44).

Also summarized in Table 1 are the quantum yields (QY) of the secondary RP for the different reconstituted samples. These values are calculated with eq 25 of ref 8 and are in reasonable agreement with values measured in ref 16.

To reduce the number of free parameters for the simulations, the dipolar ($D_{PQ}$) and exchange ($J_{PQ}$) interactions between $P^{+\bullet}$ and $Q_A^{-\bullet}$ were determined with ESEEM spectroscopy. Analytical expressions reveal contributions of both the primary and secondary RP to the out-of-phase electron spin−echo during sequential electron transfer.[45] Our delay after the laser flash, however, was long enough (~1 $\mu$s) to exclude significant effects of the primary RP on the ESEEM spectrum; at such delays, the spectrum is dominated by the spin−spin interactions of the secondary RP. Thus, the modulations observed in the time domain (Figure 3) are induced by spin−spin coupling interactions between $P^{+\bullet}$ and $Q_A^{-\bullet}$, which after Fourier transformation are determined with the equations[46]

$$D_{PQ} = 1/2(\nu_\perp - \nu_{||}) \qquad \text{and} \qquad J_{PQ} = 1/6(2\nu_\perp + \nu_{||}) \quad (1)$$

where the two characteristic frequencies $\nu_\perp$ and $\nu_{||}$ (see Figure 3) correspond to perpendicular and parallel orientations of the RP with respect to the magnetic field. The $D_{PQ}$ values thus determined showed remarkably little variation ($-0.13 < D_{PQ} < -0.12$ mT, error $\pm 0.01$ mT) for the different quinones (see Table 1) and were used without change for the simulations. Apparent $J_{PQ}$ values calculated from the Fourier transformed ESEEM spectra were $-11 \pm 3$ $\mu$T, $-12 \pm 3$ $\mu$T, and $-10 \pm 3$ $\mu$T for UQ-10, DQ, and AQ, respectively. These values were not used, however, for the simulations since recent reports have called into question the validity of determining $J_{PQ}$ from the Fourier transformed ESEEM spectra (see discussion).[47]

For the photoselection experiments, the orientation of the electric vector of the laser light relative to the optical $Q_Y$ transition of the primary donor P was taken into account. The orientation of the latter was determined from simulations of the photoselected spectra. With respect to the $Q_A^{-\bullet}$ $g$-tensor frame, the $Q_Y$ vector is rotated by $\delta = 12° \pm 2°$ and $\gamma = 140° \pm 5°$ (where $\delta$ is the angle between $Q_Y$ and the $g_z$-axis and $\gamma$ is the angle between the projection of the $Q_Y$ vector on the $x-y$ plane and the $g_x$-axis), values which are in good agreement with the angles ($\delta = 7°$ and $\gamma = 125°$) obtained in ref 27. Optimal photoselection is observed by direct excitation of the $Q_Y$ transition of P at 900 nm, whereas for excitation at 820 nm, in combination with a depolarizing light guide, almost no photoselection takes place.

## 4. Discussion

In addition to the effects of the different intrinsic line widths and $g$-tensors of the different quinones, the influence of $k_Q$ on the shape of the observed $P^{+\bullet}$ $Q_A^{-\bullet}$ ESP spectra is considerable (Figure 4). It is clearly visible that, with decreasing $k_Q$, the intermediate RP $P^{+\bullet}$ $\Phi_A^{-\bullet}$ is increasingly involved in the observed ESP spectrum. The resulting changes of the intensities of the negative and positive transitions of the two RP antiphase doublets (see Figure 5 and Scheme 1) severely affect their extensive cancellation, especially at X- and Q-band frequencies, with drastic effects on the shape and intensity of the observed ESP spectrum. This strong influence enabled us to determine accurately the decay rates of $P^{+\bullet}$ $\Phi_A^{-\bullet}$ for the different $Q_A$-reconstituted samples. Figure 4 shows that the intensity of the simulated ESP spectra increases when $k_Q$ becomes smaller. For small values of $k_Q$ ($<10^7$ $s^{-1}$), the intensity increase is diminished by a decrease of the quantum yield QY of the secondary RP,[8] as shown in Figure 5. The amplitude difference for the transitions $I_{12}$ and $I_{34}$ (Scheme 1) increases at higher EPR frequencies due to an increase in $Q_1$, the difference in Larmor frequencies of $P^{+\bullet}$ and $\Phi_A^{-\bullet}$ in the absence of spin−spin interactions. In other words, the sequential transfer mechanism becomes increasingly important at higher fields because of stronger singlet−triplet mixing in the primary RP due to the difference in Zeeman interaction between $P^{+\bullet}$ and $\Phi_A^{-\bullet}$.[11] As a result, the final shape of the observed ESP spectrum is dominated by only two transitions ($I_{12}$ and $I_{24}$). This phenomenon is demonstrated in Figure 4 where the complicated calculated line shape of the Q-band spectrum for UQ-10, AEAEA (A = absorption; E = emission), for smaller $k_Q$ far more rapidly changes to an intense, almost structureless EA line than does the line shape of the corresponding X-band spectrum. This rapid change in line shape is even more pronounced at D-band frequency (not shown). Note that the line shape of the simulated ESP spectra hardly changes with $k_Q$ when $k_Q$ becomes larger than $1 \times 10^9$ $s^{-1}$.

**Orientation of the *g*-Tensor.** For simulating all X-, Q-, and D-band ESP spectra orientation II of the $g$-tensor of $P^{+\bullet}$ was used.[34] Earlier, application of orientation II was successful for simulating high-frequency (95 GHz) ESP spectra,[38] but not for X- and K-band ESP spectra, which could be simulated satisfactorily only for orientation I.[35−37] In contrast, we have been able to simulate the X-band ESP spectra quite well for orientation II as well, by taking into account transfer of spin-correlation between the primary and secondary RP, magneto-photoselection, and by introducing small exchange interactions between $P^{+\bullet}$ and $Q_A^{-\bullet}$ (see Table 1 and below). This result provides additional support for the choice of orientation II for the $g$-tensor of $P^{+\bullet}$.

**TABLE 1: Simulation Parameters for X- (9.31 GHz), Q- (34.68 GHz), and D-band (130.0 GHz) $P^{+\bullet}$ $Q_A^{-\bullet}$ ESP Spectra**

| $Q_A$ | $g_{xx}$ ($\pm$0.0001) | $g_{yy}$ ($\pm$0.0001) | $g_{zz}$ ($\pm$0.0001) | $\Delta B_Q$ (mT) | $J_{P\Phi}$ (mT) | $J_{PQ}$ ($\mu$T) | $D_{PQ}$ (mT) | $k_T$ ($s^{-1}$) | $k_Q$ ($s^{-1}$) | QY[a] |
|---|---|---|---|---|---|---|---|---|---|---|
| UQ-10 | 2.0067 | 2.0054 | 2.0022 | $0.65 \pm 0.05$ | $-0.7 \pm 0.5$ | $-0.5 \pm 0.3$ | $-0.12 \pm 0.01$ | $(5 \pm 2) \times 10^8$ | $(5 \pm 2) \times 10^9$ | 0.99 |
| DQ | 2.0064 | 2.0051 | 2.0022 | $1.04 \pm 0.05$ | $-0.9 \pm 0.1$ | $-0.2 \pm 0.1$ | $-0.13 \pm 0.01$ | $(2 \pm 1) \times 10^8$ | $(3 \pm 1) \times 10^8$ | 0.97 |
| AQ | 2.0056 | 2.0049 | 2.0022 | $0.45 \pm 0.05$ | $-0.9 \pm 0.1$ | $-0.5 \pm 0.2$ | $-0.13 \pm 0.01$ | $(2 \pm 1) \times 10^8$ | $(3 \pm 1) \times 10^7$ | 0.75 |

$D_{P\Phi} = -0.5$ mT; $\Delta B_P = 0.95 \pm 0.05$ mT; For $\Phi_A$: $g_{iso} = 2.0035$
For P: $g_{xx} = 2.0033 \pm 0.0001$, $g_{yy} = 2.0024 \pm 0.0001$, $g_{zz} = 2.0021 \pm 0.0001$
$P^{+\bullet}\Phi_A^{-\bullet}$ singlet state decay rate: $k_S = 1.0 \times 10^7$ $s^{-1}$
$Q_Y$ transition of P relative to magnetic axes of $Q_A$: $\delta = 12 \pm 2°$ and $\gamma = 140 \pm 2°$
P, $\Phi_A$, and $Q_A$ angles are obtained from the crystal structure P4RCR[40]

[a] From eq 25 of ref 8.

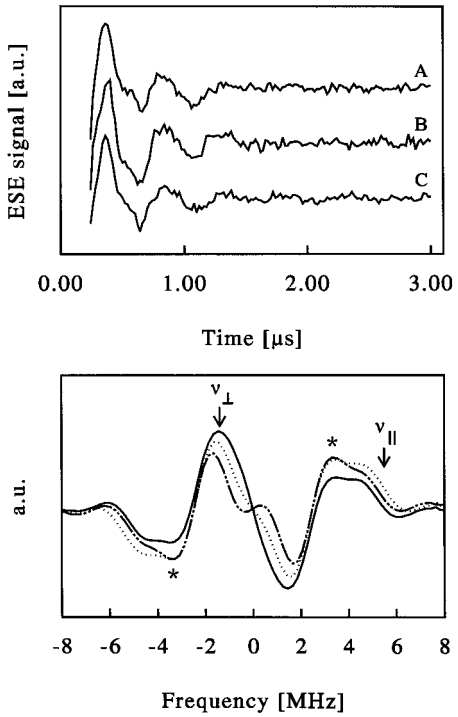


**Figure 3.** ESEEM time-domain traces (upper panel) and frequency-domain traces (lower panel) recorded for (A and solid line) UQ-10, (B and dotted line) 2-ethyl anthraquinone, and (C and dashed line) duroquinone-reconstituted, Zn-containing RCs. $T = 100$ K. The asterisks in the Fourier transformed spectra indicate possible nuclear ESEEM features.

**Dipolar Interactions.** The near identical values of the dipolar interaction between $P^{+\bullet}$ and $Q_A^{-\bullet}$ for the various quinone-reconstituted RCs, $D_{PQ} = -0.12 \pm 0.01$ mT corresponding to a distance of $28.5 \pm 0.8$ Å, indicate that the quinones are reconstituted in a position similar to that of the native UQ-10; the dipolar interaction for the nonreconstituted sample is $-0.12 \pm 0.01$ mT.[45] For UQ-10, it was shown that the quinone is hydrogen bonded to the histidine M219 and alanine M260,[20,48] and an active role of these ligating residues in effective electron transfer was suggested.[49] Likely, also for DQ and AQ the carbonyl oxygens fix the position of the quinones. For optimal simulation of the DQ spectra, we had to rotate the DQ molecule about $10° \pm 2°$ around its $g_{xx}$-axis and $5° \pm 2°$ around the $g_{yy}$-axis, compared to the position of native UQ-10. The fact that DQ lacks a long isoprenoid tail and has a relatively small size may explain this slightly different orientation. We note that, for quinone-reconstituted plant Photosystem I (PS I) particles, nearly identical distances between $P^{+\bullet}$ and $Q^{-\bullet}$ ($\equiv A_1^{-\bullet}$) were observed for various reconstituted quinones (the dipolar interaction varied little from $-0.170$ to $-0.164 \pm 0.004$ mT[50,51]), while the orientations of the assorted quinones are quite different.[25] Apparently, the native $A_1$ binding pocket in PS I is less selective than the $Q_A^{-\bullet}$ binding pocket in bacterial RCs, allowing far more freedom of rotation of the quinones. For Zn-replaced spinach PS II core particles, Hara et al. derived from ESEEM spectra a $D_{PQ}$ of $0.142 \pm 0.004$ mT,[52] corresponding to a distance of $26.9 \pm 1.0$ Å.

Following ref 53, we introduced in the ESP spectral simulations a dipolar interaction of $-0.5$ mT between $P^{+\bullet}$ and $\Phi_A^{-\bullet}$. The influence of this interaction on the simulated ESP spectra, however, is small.

**Exchange Interaction $J_{PQ}$.** The magnitude of the exchange interaction between $P^{+\bullet}$ and $Q_A^{-\bullet}$, $J_{PQ}$, is difficult to derive from the Fourier transformed ESEEM traces. The spectral features ($\nu_\perp$ and $\nu_{||}$) from which it is calculated are close to the zero-frequency region and may as a consequence be obscured by imperfect dead-time extrapolation of the echo modulation. Linebroadening produced by damping of the echo modulations may also interfere with the determination of $J_{PQ}$. Another point of concern is the effect of the finite lifetime of $P^{+\bullet}$ $\Phi_A^{-\bullet}$ on the modulation pattern of $P^{+\bullet}$ $Q_A^{-\bullet}$.[45] ESEEM spectra, however, are in comparison with ESP spectra, where cancellation effects play an important role, far less sensitive to the presence of a long-lived primary RP. Because no strong damping or line-broadening effects have been observed in the ESEEM traces for the different quinone-reconstituted samples, we have ignored the influence of the primary RP on the pulsed experiments.

Timmel et al.[47] and Dzuba[54] have shown with model calculations that the determination of the exchange interaction $J_{PQ}$ may be hampered by nuclear ESEEM. For example, the features highlighted with an asterisk in Figure 3 may originate from nuclear ESEEM modulations. Neglect of nuclear modulations in the interpretation of the Fourier transformed ESEEM could lead to overestimation of $|J_{PQ}|$ and may explain the fact that the exchange interactions calculated from the Fourier transformed ESEEM traces are over 10 times larger than those resulting from the ESP simulations, viz. $-0.5 \pm 0.3$ $\mu$T, $-0.2 \pm 0.1$ $\mu$T, and $-0.5 \pm 0.2$ $\mu$T for UQ-10, AQ, and DQ, respectively (Table 1). In PS I too, the magnitude of the exchange interaction between $P^{+\bullet}$ and $A_1^{-\bullet}$ determined with ESEEM, $J_{PA} = 0.0010 \pm 0.0015$ mT,[51] appears to have been overestimated considerably. Recently, Tang[39] has reexamined the interpretation of ESP spectra of Zn-substituted RCs of *Rb. sphaeroides* R26 by simultaneously fitting (without accounting for magnetophotoselection) six different published transient EPR spectra at three different microwave frequencies and concluded that no exchange coupling between $P^{+\bullet}$ and $Q_A^{-\bullet}$ is needed to obtain reasonable fits. In these simulations, however, the principal $g$-values of $P^{+\bullet}$ and $Q_A^{-\bullet}$ were adjusted for optimizing the fits. Such a procedure, we feel, introduces additional fit parameters without justification; the adjustments of the principal $g$-values used for the simulations considerably exceed their estimated experimental errors.[34,42] Van den Brink et al.[35] introduced a nonzero $J_{PQ}$ ($-0.8 \pm 0.2$ $\mu$T) for native RCs of

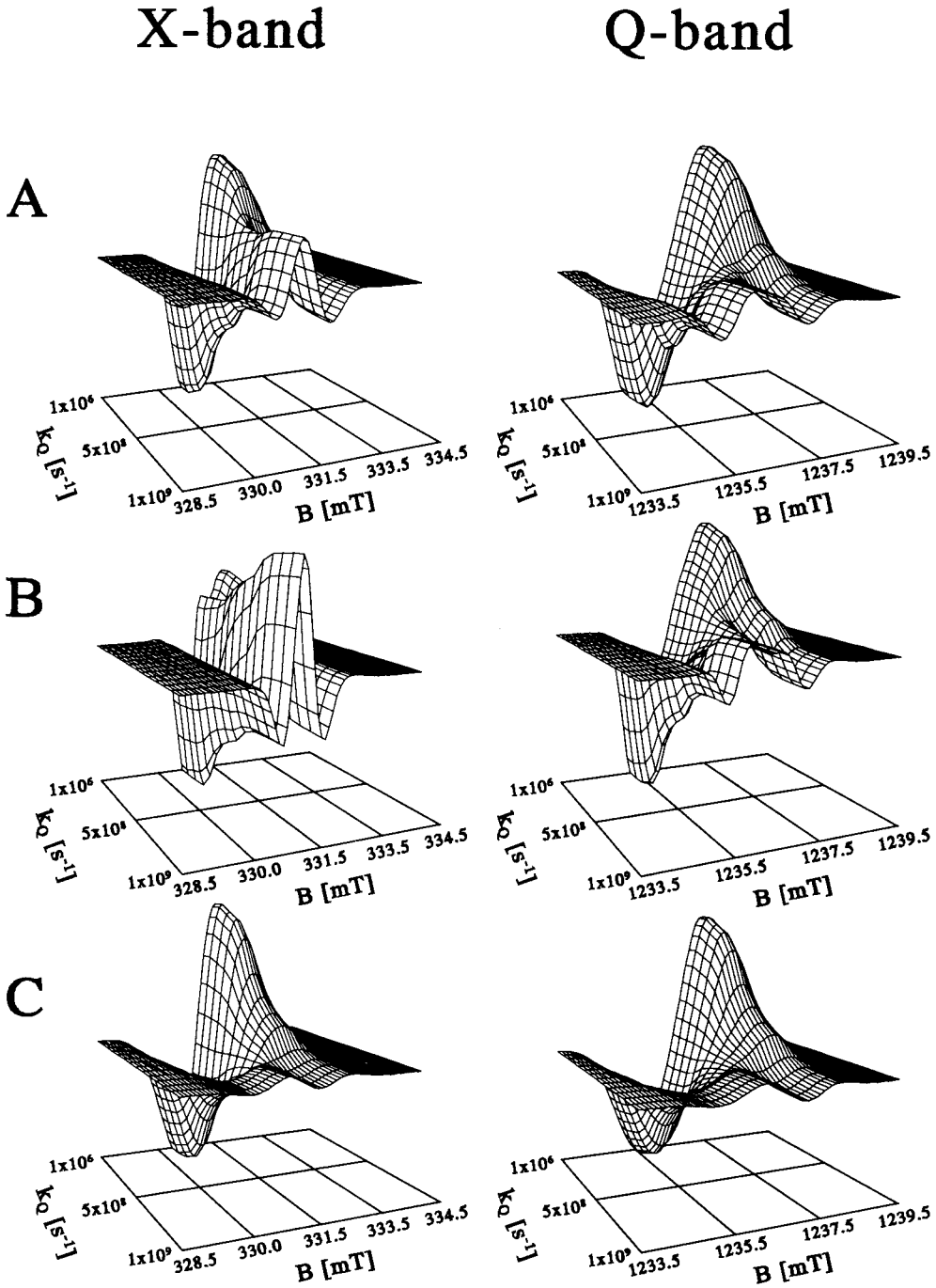


**Figure 4.** Simulated $k_Q$ dependence of the $P^{+\bullet}$ $Q_A^{-\bullet}$ ESP spectrum at X- and Q-band frequencies for (A) UQ-10, (B) 2-ethyl anthraquinone, and (C) duroquinone-reconstituted, Zn-containing RCs.

*Rb. sphaeroides* and reported a change of magnitude and sign of the exchange interaction between $P^{+\bullet}$ and $Q_A^{-\bullet}$ for menaquinone-reconstituted Zn-containing RCs ($J_{PQ} = +0.3 \pm 0.2$ $\mu$T). In their work, however, selective laser excitation of the sample was used, and because the effect of magnetophotoselection was not taken into account, the sign reversal of $J_{PQ}$ may have resulted from a photoselection artifact.[27] All considered, we feel that the values for $J_{PQ}$ determined by the ESP simulations with proper accounting for photoselection effects are more reliable than those obtained from ESEEM via eq 1 and that they represent a true measure of the exchange coupling between $P^{+\bullet}$ and $Q_A^{-\bullet}$.

It is instructive to compare our values of $J_{PQ}$ (see Table 1) with values expected on the basis of the empirical distance relation for electron-transport matrix elements proposed by Moser et al.:[55] $V_r^2 = V_0^2 \exp(-\beta r)$ or $\ln[J(r_1)/J(r_2)] = -\beta \Delta r$, with $\beta \approx 1.33$ Å$^{-1}$, $J(r) \propto V(r)$ and $r = r_1 - r_2$. The edge-to-edge distance between P and $\Phi_A$ is 9.5 Å, that between P and $Q_A$ is 22.4 Å, while $J_{P\Phi} = -0.7$ mT. Substituting these values in the distance relation yields $J_{PQ} = 2.5 \times 10^{-11}$ T. When not the relation averaged for many protein electron transport reactions is taken but one that connects two known recombination kinetics in RCs of *Rb. sphaeroides* or *Rhodopseudomonas viridis* ($\beta \approx 1.22$ Å$^{-1}$), the result is little different: $J_{PQ} = -1.0 \times 10^{-10}$ T. Both calculated values are much lower than the value determined from the ESP spectra, $J_{PQ} \approx -0.3$ $\mu$T. The value of $\beta$, however, is all-important for the outcome of this exercise. Recently, $\beta$ was found to be 0.7 Å$^{-1}$ for hole transport in DNA;[56] this value gives $J_{PQ} = -0.08$ $\mu$T, close to our experimental value. A discussion of the distance dependence

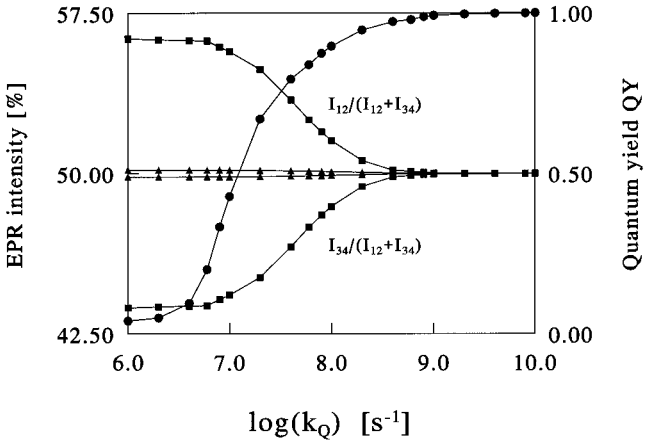


**Figure 5.** Calculated dependence of the EPR intensities ($I_{12}$, $I_{34}$) and quantum yield (QY, ●) of $P^{+\bullet}Q_A^{-\bullet}$ as a function of the rate of its formation ($k_Q$) from the intermediate RP $P^{+\bullet}\Phi_A^{-\bullet}$ at X- (▲) and Q-band (■) frequencies for UQ-10 containing RCs. See Table 1 for the parameters used.

of weak exchange interactions in copper(II) compounds is given by Hoffman et al.[57] Here, a limiting relation $|J_{lim}| = 5.9 \exp(-0.335r)$ ($J$ in $cm^{-1}$, $r$ in Å) is proposed, which for $r = 28$ Å leads to $|J_{lim}| = 0.00050$ $cm^{-1}$ (~0.50 mT) comparable with the measured exchange interaction of 0.00035 $cm^{-1}$ (~0.35 mT) for a 23−28 Å distance organic biradical (entry 27 in Table 1 of ref 57). For the P−$Q_A$ edge-to-edge distance of 22.4 Å, the relation gives $|J_{PQ,lim}| = 3.3$ mT, considerably larger than our experimental value. We conclude that within the uncertainties of experimental and theoretical work on magnetic superexchange in organic media, our measured value for $J_{PQ}$ is not unreasonable.

**Exchange Interaction $J_{P\Phi}$.** The exchange interaction between $P^{+\bullet}$ and $\Phi_A^{-\bullet}$ has proven difficult to detect in native RCs, mainly because of the short lifetime of this RP state (200 ps). The application of RYDMR/MARY (magnetic field dependence of the reaction yield)[44] or fast ESP[53,58] spectroscopy allows one to determine $|J_{P\Phi}|$ indirectly or directly in $Q_A$-reduced or $Q_A$-depleted RCs. The sign of $J_{P\Phi}$ has been debated heavily during the past years. Recent experiments and simulations of the ESP spectrum of the primary RP in the native system indicated that $J_{P\Phi}$ is negative.[53,58] Our experiments provide indirect information about $J_{P\Phi}$ from the easily observable $P^{+\bullet}Q_A^{-\bullet}$ ESP spectrum. From its spectral simulation, a $J_{P\Phi}$ of $-0.9 \pm 0.1$ mT was found for both the DQ- and AQ-reconstituted samples. For the UQ-10 reconstituted sample, due to the relatively fast electron-transfer rate between $\Phi_A^{-\bullet}$ and $Q_A$, the observed ESP spectrum is barely affected by changes of magnitude of $J_{P\Phi}$ as shown in Figure 6A. Thus, the pronounced effect of the magnitude of $J_{P\Phi}$ on the shape of the simulated ESP spectrum for small values of $k_Q$ is strongly reduced for large $k_Q$'s, affecting the accuracy of $J_{P\Phi}$ for UQ-10-containing RCs, viz. $J_{P\Phi} = -0.7 \pm 0.5$ mT. This value is in good agreement with the most recent value of $J_{P\Phi}$ in native RCs ($-0.7 \pm 0.2$ mT[53,58]).

The influence of the magnitude of $k_Q$ and of the sign and magnitude of $J_{P\Phi}$ on the shape of simulated Q-band ESP spectra of AQ-reconstituted RCs is shown in parts A and B of Figure 6. The spectrum inverts as $J_{P\Phi}$ changes sign, and the deviations from the experimental line shape increase appreciably when the magnitude of $J_{P\Phi}$ is enlarged or $k_Q$ is decreased. The influence of the magnitude of $J_{P\Phi}$ becomes even stronger at higher magnetic field values as a result of enhanced singlet−triplet mixing in the $P^{+\bullet}\Phi_A^{-\bullet}$ RP state (Figure 6C).

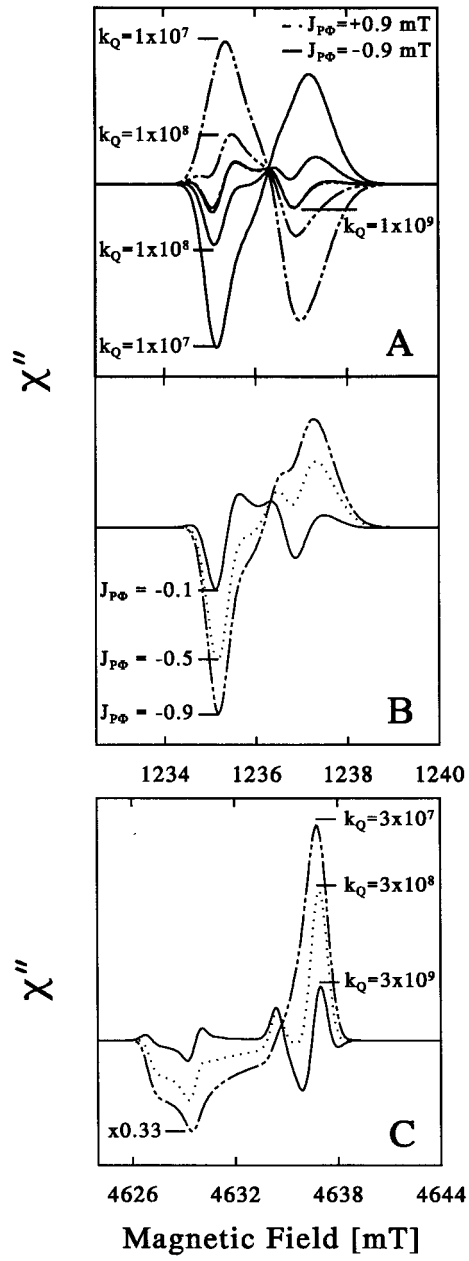


**Figure 6.** The influence of the sign of $J_{P\Phi}$ (+0.9 mT, dashed lines; −0.9 mT, solid lines) for several $k_Q$ values in $s^{-1}$ (A) and the magnitude of $J_{P\Phi}$ (mT) for $k_Q = 3 \times 10^7$ $s^{-1}$ (B) on the shape of simulated Q-band ESP spectra of AQ-reconstituted RCs or on the D-band ESP spectrum of UQ-10 (C); for the simulation parameters, see Table 1.

**Kinetics of the Primary RP State.** At D-band frequency, there is almost no cancellation of the two anti-phase doublets (Scheme 1), and as a result, the ESP spectrum is far less sensitive to changes in the dipolar, exchange, and hyperfine interactions. Therefore, at D-band frequency the effect of altered $k_Q$ rates on the shape of the ESP spectrum dominates over possible changes in the other parameters. Figure 6C shows D-band simulations for UQ-10 reconstituted RCs for three different $k_Q$ rates; the other parameters were kept fixed to that of UQ-10 RCs. For $k_Q = 3 \times 10^9$ $s^{-1}$, the simulation resembles the experimental ESP spectrum for UQ-10 RCs. For $k_Q = 3 \times 10^8$ $s^{-1}$, similar to the rate for DQ-reconstituted RCs,[10,16] the simulated line shape closely approaches, despite the different $g$-values and line width parameters (which correspond to UQ-RCs), the line shape features of the experimental spectrum for DQ-RCs. For $k_Q = 3 \times 10^7$ $s^{-1}$, similar to the rate for AQ-

RCs,[10,16] the experimental spectrum of AQ-reconstituted RCs is obtained. Note the rapid increase of ESP intensity with the decreasing value of $k_Q$. The ESP spectra at the three frequencies were recorded at different temperatures. Since $k_Q$ and QY are only weakly dependent on temperature ($14 < T < 295$ K),[16] we have ignored their temperature variation. Our experimental results and simulations show that high-frequency ESP allows one also to determine accurately the $k_Q$ rate of electron transfer between $\Phi_A^{-\bullet}$ and $Q_A$, for different types of quinone in the $Q_A$ pocket.

The simulation of the ESP spectra is sensitive to the value of $k_T$ only when $k_Q$ is relatively small. For UQ-10 RCs (high $k_Q$), we used $k_T$ obtained from $P^{+\bullet}\,\Phi_A^{-\bullet}$ ESP experiments with native RCs ($k_T = (5-9) \times 10^8$ s$^{-1}$).[44,53] For the DQ- and AQ-reconstituted low $k_Q$ RCs, the simulations allowed us to determine $k_T$ quite accurately, $k_T = (2 \pm 1) \times 10^8$ s$^{-1}$ (Table 1). This value is in the low range of literature values obtained for native samples ($(1-10) \times 10^8$ s$^{-1}$ at various temperatures and external magnetic fields). The variation in the latter values is probably related to the energetic inhomogeneity of the $P^{+\bullet}\,\Phi_A^{-\bullet}$ state.[59] All simulations were relatively insensitive to changes of $k_S$. Within the accuracy of the experiments, we did not observe a magnetic field effect on the decay rates of the RP states.

**Comparison with Other Sequential Electron Transfer Models.** Simulations by Tang et al.[11] employing a positive $J_{P\Phi}$ of 0.7 mT in a parameter set adapted to *Rb. sphaeroides* showed an increased effect of sequential electron transfer at very high magnetic fields (8.9 T) for relatively large $k_Q$ values ($6.7 \times 10^9$ and $3.3 \times 10^9$ s$^{-1}$). The enhanced effect of sequential electron transfer is due to the increased contribution of the $\Delta g$ term in the singlet−triplet mixing of the primary RP. The case of quinone-modified RCs with smaller $k_Q$'s and attendant strong line shape changes, however, was not treated. A similar parameter set was used by Utschig et al. to simulate X- and Q-band spectra of $Fe^{2+}$-removed RCs of *Rb. sphaeroides*.[14] The prolonged $P^{+\bullet}\,\Phi_A^{-\bullet}$ lifetime of 3−6 ns measured in these $Fe^{2+}$-modified RCs is still too fast, however, to see a pronounced effect of sequential electron transfer at these EPR frequencies. In both studies, no direct comparison with experimental spectra was made. We have reproduced the simulations of ref 11 and find that, for small $k_Q$, as in quinone-modified Zn-substituted RCs, the parameter set of ref 11 cannot reproduce the experimental ESP spectra. Notably, $J_{P\Phi} > 0$ leads to simulated ESP spectra that are inverted with respect to the experimental spectra (see also Figure 6A).

Morris et al. applied a sequential model to fit experimental ESP spectra of quinone-reconstituted, $Fe^{2+}$-containing RCs,[10] however, without taking into account the magnetic coupling between $Q_A^{-\bullet}$ and $Fe^{2+}$. Again, a positive $J_{P\Phi}$, in combination with a relatively large positive $J_{PQ}$ value of 2.5 $\mu$T, was used for the simulations. We have globally reproduced the simulations presented in ref 10 and find that for the parameter set in ref 10 the line shapes of the simulated spectra do not critically depend on the sign of $J_{P\Phi}$. However, when the coupling between Q and $Fe^{2+}$ is correctly introduced, as in ref 24, the simulated line shapes of the ESP spectra of $Fe^{2+}$-containing RCs are drastically altered and can only be reproduced for $J_{P\Phi} < 0$. Reassuringly, with our parameter set and the *g*-matrixes of the $(Fe^{2+}Q_A^{-\bullet})$ complex in ref 24, simulations are achieved that are virtually identical to the experimental ESP spectra of $Fe^{2+}$-containing RCs presented in ref 10.

## 5. Conclusions and Prospects

In the present work, we show that the combination of quinone modification and very high frequency EPR is a powerful tool for accurately determining the magnetic interactions between photoionized electron transport cofactors. An enhanced effect of transfer of spin correlation from the primary RP $P^{+\bullet}\,\Phi_A^{-\bullet}$ to the secondary RP $P^{+\bullet}\,Q_A^{-\bullet}$ has been achieved by replacing the native UQ-10 quinone with other quinones, thus slowing down the forward electron-transfer rate from $\Phi_A^{-\bullet}$ to $Q_A$. We have successfully used the theoretical description by Hore[8] of the effect of sequential electron transfer on SCRP, for simulating the observed multifrequency SCRP $P^{+\bullet}\,Q_A^{-\bullet}$ ESP spectra of a variety of quinone-substituted Zn-containing RCs of *Rb. sphaeroides* R26. All spectra at X-, Q-, and D-band frequency were simulated with orientation II for the *g*-tensor of $P^{+\bullet}$, providing additional support that this orientation is indeed the correct one. The use of multifrequency ESP appreciably improved the accuracy of determining the exchange interaction between $P^{+\bullet}$ and $\Phi_A^{-\bullet}$, $J_{P\Phi}$, and the kinetics of the primary RP. $J_{P\Phi}$ was found to be $-0.9 \pm 0.1$ mT for DQ- and AQ-reconstituted RCs, not significantly different from the value of $-0.7 \pm 0.5$ mT obtained for the UQ-10 reconstituted sample. For an accurate determination of the dipolar interaction between $P^{+\bullet}$ and $Q_A^{-\bullet}$, the out-of-phase ESEEM technique is better suited than ESP (which is relatively insensitive to $D_{PQ}$). $D_{PQ}$ proved remarkably constant for the different quinones, $-0.12 \pm 0.01$ mT. The magnitude of the exchange interaction between $P^{+\bullet}$ and $Q_A^{-\bullet}$ is difficult to obtain from ESEEM spectroscopy; our ESP results convincingly show that it is small but nonzero, $J_{PQ} = -0.5 \pm 0.3$ $\mu$T, $-0.2 \pm 0.1$ $\mu$T, and $-0.5 \pm 0.2$ $\mu$T for UQ-10, AQ, and DQ, respectively.

We anticipate that the approach of multifrequency ESP in combination with quinone replacement may be fruitfully applied to plant material. In PS I, the quinone $A_1$ can be readily replaced by other quinones and the $P^{+\bullet}\,A_1^{-\bullet}$ ESP spectrum can be easily detected. The lifetime of the precursor $P^{+\bullet}\,A_0^{-\bullet}$ RP state is too short to induce singlet−triplet mixing (35 ps). Prolongation of the $P^{+\bullet}\,A_0^{-\bullet}$ RP lifetime by reconstitution of $A_1$ with different quinones may induce changes in the observed ESP spectrum and may therefore yield information about the magnetic interactions between $P^{+\bullet}$ and $A_0^{-\bullet}$, in particular for high-field ESP, which as we have shown is very sensitive to changes in the rate of electron transfer between the succeeding RP cofactors in the RC. Likewise, we expect that high-field ESP measurements will resolve the uncertainties concerning the presence of an intermediate $P^{+\bullet}\,A_1^{-\bullet}$ RP state in the PS I type RCs of heliobacteria and green sulfur bacteria (see ref 60). We note that a pronounced effect of transfer of spin-correlation from the $P^{+\bullet}\,A_1^{-\bullet}$ RP (lifetime $\sim$280 ns[61]) to the subsequent $P^{+\bullet}\,(FeS)^{-\bullet}$ RP has been observed in the ESP spectrum of the latter.[61,62] Multifrequency ESP will also yield valuable information about the primary charge-separation processes and cofactor interactions for PS II.

**Acknowledgment.** We thank Mr. A. H. M. de Wit for growing the bacteria, Ms. S. J. Jansen for help with preparing the RCs, and Drs. I. I. Proskuryakov, P. J. Hore, C. R. Timmel, and M. C. Thurnauer for valuable discussions. This research was supported by the Earth and Life Sciences (ALW) section of The Netherlands Organization for Scientific Research (NWO).

## References and Notes

(1) Hoff, A. J.; Deisenhofer, J. *Phys. Rep.* **1997**, *287*, 2.
(2) Angerhofer, A.; Bittl, R. *Photochem. Photobiol.* **1996**, *63*, 11.

(3) Hore, P. J.; Hunter, D. A.; McKie, C. D.; Hoff, A. J. *Chem. Phys. Lett.* **1987**, *137*, 495.
(4) Closs, G. L.; Forbes, M. D. E.; Norris, J. R. *J. Phys. Chem.* **1987**, *91*, 3592.
(5) Bixon, M.; Jortner, J.; Michel-Beyerle, M. E. *J. Phys. Chem.* **1993**, *180*, 193.
(6) Bixon, M.; Jortner, J.; Michel-Beyerle, M. E. *Chem. Phys.* **1995**, *197*, 389.
(7) Okamura, M. Y.; Fredkin, D. R.; Isaacson, R.; Feher, G. In *Tunneling in Biological Systems*; Chance, B., DeVault, D. C., Frauenfelder, H., Marcus, R., Schrieffer, J. R., Sutin, N., Eds.; Academic Press: New York, 1979; p 729.
(8) Hore, P. J. *Mol. Phys.* **1996**, *89*, 1195.
(9) Norris, J. R.; Morris, A. L.; Thurnauer, M. C.; Tang, J. *J. Chem. Phys.* **1990**, *92*, 4239.
(10) Morris, A. L.; Snyder, S. W.; Zhang, Y.; Tang, J.; Dutton, P. L.; Robertson, D. E.; Gunner, M. R.; Thurnauer, M. C. *J. Phys. Chem.* **1995**, *99*, 3854.
(11) Tang, J.; Bondeson, S.; Thurnauer, M. C. *Chem. Phys. Lett.* **1996**, *253*, 293.
(12) Snyder, S. W.; Morris, A. L.; Bondeson, S. R.; Norris, J. R.; Thurnauer, M. C. *J. Am. Chem. Soc.* **1993**, *115*, 3774.
(13) Kirmaier, C.; Holten, D.; Debus, R. J.; Feher, G.; Okamura, M. Y. *Proc. Natl. Acad. Sci. U.S.A.* **1986**, *83*, 6407.
(14) Utschig, L. M.; Greenfield, S. R.; Tang, J.; Laible, P. D.; Thurnauer, M. C. *Biochemistry* **1997**, *36*, 8548.
(15) Liu, B. L.; Van Kan, P. J. M.; Hoff, A. J. *FEBS Lett.* **1991**, *289*, 23.
(16) Gunner, M. R.; Dutton, P. L. *J. Am. Chem. Soc.* **1989**, *111*, 3400.
(17) Gunner, M. R.; Robertson, D. E.; LoBrutto, R. L.; McLaughlin, A. C.; Dutton, P. L. In *Progress in Photosynthesis Research*; Biggins, J., Ed.; Martinus Nijhof: Dordrecht, 1986; Vol. I, p 217.
(18) Laible, P. D.; Zhang, Y.; Morris, A. L.; Snyder, S. W.; Ainsworth, C.; Greenfield, S. R.; Wasielewski, M. R.; Parot, P.; Schoepp, B.; Schiffer, M.; Hanson, D. K.; Thurnauer, M. C. *Photosynth. Res.* **1997**, *52*, 93.
(19) Kirmaier, C.; Gaul, D.; Debey, R.; Holten, D.; Schenck, C. C. *Science* **1991**, *251*, 922.
(20) Spoyalov, A. P.; Hulsebosch, R. J.; Shochat, S.; Gast, P.; Hoff, A. J. *Chem. Phys. Lett.* **1996**, *263*, 715.
(21) Woodbury, N. W.; Parson, W. W.; Gunner, M. R.; Prince, R. C.; Dutton, P. L. *Biochim. Biophys. Acta* **1986**, *851*, 6.
(22) Gunner, M. R.; Robertson, D. E.; Dutton, P. L. *J. Phys. Chem.* **1986**, *90*, 3783.
(23) Proskuryakov, I. I.; Klenina, I. B.; Shkuropatov, A. Ya.; Shkuropatova, V. A.; Shuvalov, V. A. *Biochim. Biophys. Acta* **1993**, *1142*, 207.
(24) Van den Brink, J. S.; Hermolle, T. E. P., Gast, P.; Hore, P. J.; Hoff, A. J. *J. Phys. Chem.* **1996**, *100*, 2430.
(25) Van der Est, A.; Sieckmann, I.; Lubitz, W.; Stehlik, D. *Chem. Phys.* **1995**, *194*, 349.
(26) Stehlik, D.; Bock, C. H.; Petersen, J. *J. Phys. Chem.* **1989**, *93*, 1612.
(27) Proskuryakov, I. I.; Klenina, I. B.; Borovykh, I. V.; Gast, P.; Hoff, A. J. *Chem. Phys. Lett.* **1998**, *299*, 566.
(28) Okamura, M. Y.; Isaacson, R. A.; Feher, G. *Proc. Natl. Acad. Sci. U.S.A.* **1975**, *72*, 3491.
(29) Tiede, D. M.; Dutton, P. L. *Biochim. Biophys. Acta* **1981**, *637*, 278.
(30) Bosch, M. K. Doctoral Thesis, Leiden University, The Netherlands, 1995; p 8.
(31) Salikhov, K. M.; Kandrashkin, Yu. E.; Salikhov, A. K. *Appl. Magn. Res.* **1992**, *3*, 199.
(32) Tang, J.; Thurnauer, M. C.; Norris, J. R. *Chem. Phys. Lett.* **1994**, *219*, 283.
(33) Dzuba, S. A.; Gast, P.; Hoff, A. J. *Chem. Phys. Lett.* **1995**, *236*, 595−602.
(34) Klette, R.; Törring, J. T.; Plato, M.; Möbius, K.; Bönigk, B.; Lubitz, W. *J. Phys. Chem.* **1993**, *97*, 2015.
(35) Van den Brink, J. S.; Hulsebosch, R. J.; Gast, P.; Hore, P. J.; Hoff, A. J. *Biochemistry* **1994**, *33*, 13668.
(36) Füchsle, G.; Bittl, R.; Van der Est, A.; Lubitz, W.; Stehlik, D. *Biochim. Biophys. Acta* **1993**, *1142*, 23.
(37) Van der Est, A.; Bittl, R.; Abresch, E. C.; Lubitz, W.; Stehlik, D. *Chem. Phys. Lett.* **1993**, *212*, 561.
(38) Prisner, T. F.; Van der Est, A.; Bittl, R.; Lubitz, W.; Stehlik, D.; Möbius, K. *Chem. Phys.* **1995**, *194*, 361.
(39) Tang, J. *Chem. Phys. Lett.* **1998**, *290*, 49.
(40) Komiya, H.; Yeates, T. O.; Rees, D. C.; Allen, J. P.; Feher, G. *Proc. Natl. Acad. Sci. U.S.A.* **1988**, *85*, 9012.
(41) Feezel, L. L.; Gast, P.; Smith, U. H.; Thurnauer, M. C. *Biochim. Biophys. Acta* **1989**, *974*, 149.
(42) Burghaus, O.; Plato, M.; Rohrer, M.; MacMillan, F.; Lubitz, W.; Möbius, K. *J. Phys. Chem.* **1993**, *97*, 7639.
(43) Nimz, O.; Lendzian, F.; Boullais, C.; Lubitz, W. *Appl. Magn. Res.* **1998**, *14*, 2.
(44) Volk, M.; Ogrodnik, A.; Michel-Beyerle, M. E. In *Anoxygenic Photosynthetic Bacteria*; Blankenship, R. E., Madigan, M. T., Bauer, C. E., Eds.; Kluwer: Dordrecht, 1995; p 595.
(45) Jeschke, G.; Bittl, R. *Chem. Phys. Lett.* **1998**, *294*, 323.
(46) Dzuba, S. A.; Gast, P.; Hoff, A. J. *Chem. Phys. Lett.* **1997**, *268*, 273.
(47) Timmel, C. R.; Fursman, C. E.; Hoff, A. J.; Hore, P. J. *Chem. Phys.* **1998**, *226*, 271.
(48) Van den Brink, J. S.; Spoyalov, A. P.; Gast, P.; Van Liemt, W. B. S.; Raap, J.; Lugtenburg, J.; Hoff, A. J. *FEBS Lett.* **1994**, *353*, 273.
(49) Lendzian, F.; Rautter, J.; Käss, H.; Gardiner, A.; Lubitz, W. *Ber. Bunsen-Ges. Phys. Chem.* **1996**, *100*, 2036.
(50) Zech, S. G.; Van der Est, A. J.; Bittl, R. *Biochemistry* **1997**, *36*, 9774.
(51) Dzuba, S. A.; Hara, H.; Kawamori, A.; Iwaki, M.; Itoh, S.; Tsvetkov, Yu. D. *Chem. Phys. Lett.* **1997**, *264*, 238.
(52) Hara, H.; Dzuba, S. A.; Kawamori, A.; Akabori, K.; Tomo, T.; Satoh, K.; Iwaki, M.; Itoh, S. *Biochim. Biophys. Acta* **1997**, *1322*, 77.
(53) Till, U.; Klenina, I. B.; Proskuryakov, I. I.; Hoff, A. J.; Hore, P. J. *J. Phys. Chem. B* **1997**, *101*, 10939.
(54) Dzuba, S. A. *Chem. Phys. Lett.* **1997**, *278*, 333.
(55) Moser, C. C.; Keske, J. M.; Warncke, K.; Farid, R. S.; Dutton, P. L. *Nature* **1992**, *355*, 796.
(56) Meggers, E.; Michel-Beyerle, M. E.; Giese, B. *J. Am. Chem. Soc.*, in press.
(57) Hoffman, S. K.; Hilczer, W.; Goslar, J. *Appl. Magn. Reson.* **1994**, *7*, 289.
(58) Proskuryakov, I. I.; Klenina, I. B.; Hore, P. J.; Bosch, M. K.; Gast, P.; Hoff, A. J. *Chem. Phys. Lett.* **1996**, *257*, 333.
(59) Ogrodnik, A.; Keupp, W.; Volk, M.; Aumeier, G.; Micher-Beyerle, M. E. *J. Phys. Chem.* **1994**, *98*, 3432.
(60) Van der Est, A.; Hager-Braun, C.; Leibl, W.; Hauska, C.; Stehlik, D. *Biochim. Biophys. Acta* **1998**, *1409*, 87.
(61) Van der Est, A.; Bock, C.; Golbeck, J.; Brettel, K.; Sétif, P.; Stehlik, D. *Biochemistry* **1994**, *33*, 11789.
(62) Bock, C. H.; Van der Est, A. J.; Brettel, K.; Stehlik, D. *FEBS Lett.* **1989**, *247*, 91.